

Design and Implementation of High Efficiency and Broadband Transmission-Type Polarization Converter Based on Diagonal Split-Ring Resonator

Rui Zhao, Haiyan Chen*, Linbo Zhang, Fengxia Li, Peiheng Zhou,
Jianliang Xie, and Longjiang Deng

Abstract—In this paper, the design and implementation of a three-layer linear polarization converter having broadband and asymmetric transmission (AT) properties is demonstrated. A 3.2 mm thick transmission-type polarization converter with two separate operating frequency bands is obtained with a cut-wire sandwiched by two layers of diagonal split-ring resonator (DSRR). The asymmetric transmission property can be realized by rotating the upper and lower DSRR dislocation, and its physical mechanism can be explicated by the Fabry-Pérot-like interference effect. Experimental results are presented and compared to numerical simulations, and they demonstrate that the proposed polarization converter has a significantly polarization conversion ratio over 0.8 in frequency bandwidths 8–11 GHz and 17–21 GHz for the forward and backward incidences. The proposed polarization converter has a great potential to be used as an asymmetric transmission radome or diode-like device in microwave domain.

1. INTRODUCTION

Polarization, one of the most important characteristics of electromagnetic (EM) waves, plays significant roles in asymmetric transmission [1–6], antennas [7, 8], etc. Conventional devices for controlling wave polarization including birefringence materials and optically active materials are bulky, and their bandwidth is narrow. However, the devices for controlling polarization should feature the merits of compact size, broadband and high polarization conversion efficiency in practical application. Metamaterials (MMs) have attracted increasing attention for their exotic EM responses and novel physical properties which can provide unprecedented opportunities to manipulate EM characteristics [9–17], including polarization [18–27] and anomalous refraction [14, 28]. Hence, MMs-based polarization converter devices have been studied widely. Due to its asymmetric transmission effect, linear polarization converters in transmission are particularly attractive.

The asymmetric transmission phenomenon in linear polarization converter was firstly observed by Fedotov et al. [1]. After that, many methods and designs such as multi-layer MMs have been proposed to enhance the magnitude of asymmetric transmission effect [29–35]. In 2011, Kang et al. [36] proposed a S-shaped MM whose transmission polarization conversion efficiency is over 0.8 in the opposite propagation directions and exhibits an asymmetric transmission of linearly polarized waves at 6.2 GHz. And then, in 2013, Shi et al. [37] reported a bi-layered chiral MM and demonstrated to achieve cross-polarization conversion with an efficiency of over 90% for both y - and x -polarized waves. Subsequently, in 2015, cross-shaped bi-layered MM was demonstrated by Wang et al. [38, 39], and the asymmetric transmission bandwidth could be up to 33% relative the central wavelength with a efficiency of 0.6. In the same year,

Received 6 November 2017, Accepted 12 February 2018, Scheduled 28 February 2018

* Corresponding author: Haiyan Chen (chenhy@uestc.edu.cn).

The authors are with the National Engineering Research Center of Electromagnetic Radiation Control Materials, State Key Laboratory of Electronic Thin Film and Integrated Devices, University of Electronic Science and Technology of China, Chengdu 610054, China.

Serebryannikov and Mutlu proposed a subwavelength resonances in open ultrathin chiral structures, which could realize AT in different frequencies, and its bandwidth is less than 1 GHz [33]. In a word, the asymmetric transmission effect for the earlier proposed MMs-based structures is narrow band or low efficiency (usually no more than 0.6). Thus, it is desirable to design high efficiency and broadband transmission-type polarization converter.

In this work, we present a three-layer high-efficiency and broadband polarization converter which exhibits asymmetric transmission phenomenon. The electromagnetic transmission properties of the proposed structure are investigated by the finite difference time domain method. In order to validate our design, the proposed structure is fabricated using the conventional printed circuit board (PCB) process, and test is done employing free-space method in microwave anechoic chamber. Moreover, to clarify the resonant characterization, the electrical field and surface current distributions at resonant frequencies are analyzed, and the method based on the Fabry-Pérot-like resonant cavity theory is also proposed for giving a clear explanation to the physical mechanism of the high-efficiency and broadband polarization conversion. Furthermore, the incidence angle dependent stability of the proposed polarization conversion is discussed.

2. SIMULATIONS AND EXPERIMENTS

Figure 1 shows a schematic diagram of the proposed transmission-type polarization converter, which is composed of a cut-wire and sandwiched by two layers of diagonal split-ring resonator (DSRR) with different split directions. Numerical simulations were performed using commercial software CST Microwave Studio and frequency domain solver was carried out with unit cell boundary condition in the x - y directions and the Floquet ports in the z -direction to extract S parameters. The period of the unit cell p was set as 5 mm, and we could form the bottom layer by rotating the top layer 90 degrees counter clock wise. The key parameters of the unit cell were as follows: $p = l_2 = 5$ mm, $l_1 = 2.7$ mm, $a = 2$ mm, $b = 1.25$ mm, $w = 2$ mm, and $d = 3.2$ mm. The multi-layered MM by copper (conductivity = 5.96×10^7 Sm $^{-1}$) was fabricated on an FR-4 substrate with a permittivity = 4.3 and a dielectric loss tangent of 0.025. In order to experimentally verify the performance of the converter, we fabricated the structure with the dimension 300 mm \times 300 mm as shown in Fig. 1(c), containing 60×60 unit cells. The measurements are performed using an Agilent 8720ET vector network analyzer and two broadband horn antennas. By changing the orientation of the two horn antennas, all four components of the wave transmission for different polarizations were measured.

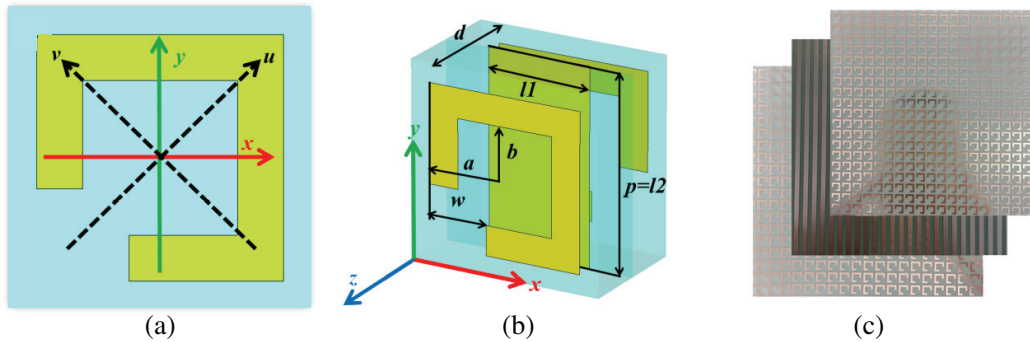


Figure 1. Schematic of the unit cell of the multi-layered linear converter. (a) Front view of the structure, (b) perspective view of the structure and (c) Photograph of the experimental sample.

In Fig. 2, we illustrate the simulated transmission coefficients in the three-layer MM for forward and backward propagating waves. The transmission of the structure can be presented in terms of complex transmission coefficients T_{ij}^d in Jones matrix, where $t_{ij}^d = |T_{ij}^d|$, the superscript d refers to the forward (along $-z$ axis) or backward (along $+z$ axis) wave propagations, the subscripts i and j correspond to the polarization states of the transmitted and incident waves, which could be either u or v linearly

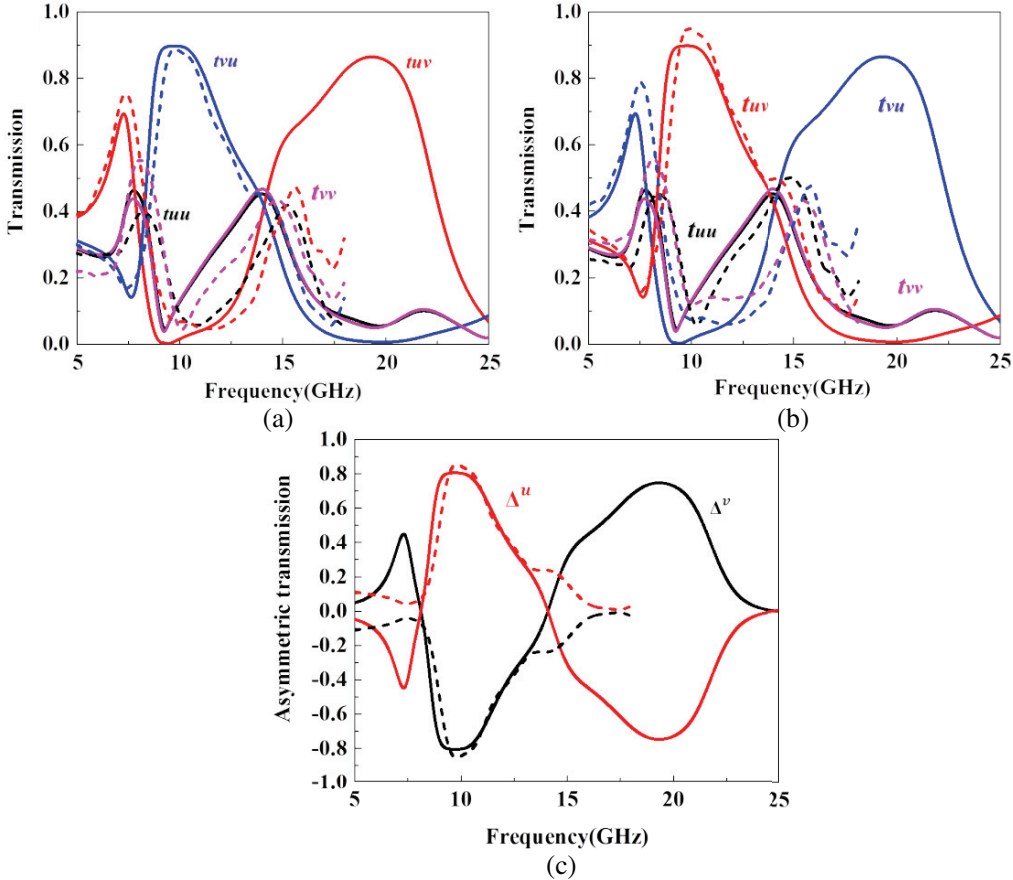


Figure 2. Transmission properties of the proposed polarization converter, solid line for simulation, dotted line for experiment. (a) and (b) represent transmission coefficients (absolute value) for forward incidence and backward incidence respectively, (c) represent asymmetric transmission coefficient calculated according to the data from (a) and (b).

polarized waves in Fig. 1(a). Under normal incidence, it is seen that the co-polarization transmission coefficient t_{vv} of v -polarized and t_{uu} of u -polarized incidence wave are exactly consistent with each other. In contrast to co-polarization transmission, the cross-polarization transmission coefficient t_{vu} of u -polarized incident wave is extremely different from t_{uv} of v -polarized incident wave in the frequency bandwidths 8–11 GHz and 17–21 GHz. Based on [36, 40], the above two conditions include ① Co-polarization transmission coefficient T_{uu} coincides well with T_{vv} . ② The cross-polarization transmission coefficient T_{uv} should be extremely different from T_{vu} at the considering frequencies, which could ensure the presence of asymmetric transmission effect for linear polarization waves only. Most interestingly, two separated passbands are observed, one for v -to- u polarization conversion and the other for u -to- v polarization conversion, which demonstrate strong optical activity in the proposed MM.

The numerical and experimental transmission coefficients are given in Figs. 2(a) and 2(b). It is obtained that $t_{uu} = t_{vv}$ and $t_{uv} \neq t_{vu}$, which means that only linear polarization conversion occurs. In Fig. 2(a), the polarization conversion bandwidth of cross-polarization transmission t_{vu} over 0.8 can be achieved from 8–11 GHz for simulations and reaches a maximum of 0.9 at 9.7 GHz while both the co-polarization transmissions t_{uu} and t_{vv} are under 0.1. In this passband, the incident u -polarized wave is almost completely transmitted to v -polarized wave while the incident v -polarized wave is completely blocked through the structure. Meanwhile, an obvious resonant peak in t_{uv} can be observed with a maximum larger than 0.87 at around 19.27 GHz and the bandwidth over 0.8 could be achieved from 17–21 GHz, where incident v -polarized wave is almost completely transmitted to u -polarized wave while incident u -polarized wave cannot pass through the structure. In addition, when the propagation

direction is reversed, t_{uv} and t_{vu} interchange with each other shown in Fig. 2(b). The measured cross-polarization transmissions are in good agreement with the simulated ones in Figs. 2(a) and (b). Due to the limitations of experimental conditions, the measurement is conducted only in the range of 5–18 GHz. Theoretical and experimental results demonstrate that the multi-layered MM is nearly transparent to incident linearly polarized waves in two separated asymmetric transmission bands, where a linear polarization wave can be completely converted to its cross-polarization and then transmitted, while the same one cannot pass through the MM in the opposite direction. The little discrepancy is caused by the fabrication error and distortion at high frequency.

3. ANALYSIS AND DISCUSSIONS

3.1. The Theoretical and Experimental Asymmetric Transmission Coefficient

The asymmetric transmission effect of the linear polarization waves is usually characterized by a symbol Δ , which is defined as the difference between the transmissions in two opposite propagation directions. The asymmetric transmission coefficients for the linear polarization waves (superscript u or v represents u -polarized waves or v -polarized waves respectively, and superscript f or b represents the forward propagation or the backward propagation respectively) are then defined as:

$$\begin{aligned}\Delta^u &= \left|T_{vu}^f\right|^2 - \left|T_{vu}^b\right|^2 = \left|T_{vu}^f\right|^2 - \left|T_{uv}^f\right|^2 \\ \Delta^v &= \left|T_{uv}^f\right|^2 - \left|T_{uv}^b\right|^2 = \left|T_{uv}^f\right|^2 - \left|T_{vu}^f\right|^2\end{aligned}\quad (1)$$

According to Eq. (1), Δ^u and Δ^v of the proposed polarization converter are presented, just as in Fig. 2(c). In particular, one can see that the asymmetry factor curves Δ^u and Δ^v show two opposite peaks located at about 9.7 and 19.27 GHz in Fig. 2(c). Two values of 0.82/−0.82 and −0.78/0.78 in the curves Δ^u and Δ^v imply that the u/v -polarized wave in the forward direction is mostly allowed/forbidden at about 9.7 GHz and forbidden/allowed at 19.27 GHz, respectively. Although the measured asymmetric transmissions in Fig. 2(c) are only in the range of 5–18 GHz, they agree very well with the simulated ones in the whole bands except some distortion at high frequency. It is clearly demonstrated that two curves Δ^u and Δ^v are exactly contrary to each other in Fig. 2(c). The slight amplitude difference in between the simulation and experiment may be caused by the mismatch between the assumed imaginary part of permittivity and the realistic material parameter.

3.2. Angle Independent of Polarization Converter

The above analysis shows that the proposed converter has advantages of dual-band and high-efficiency polarization conversion under normal incidence; however, in practical applications, the EM wave is usually incident onto converter with an oblique incident angle. Therefore, the relationship between the angle of incidence and polarization conversion performance needs to be investigated. In this section, the response of our proposed converter for oblique incident performance is examined. To this end, incident angle θ is defined as those formed between the propagation vector of the incident wave and the z -axis over xz -plane. The simulated transmittance for various angles θ is illustrated in Fig. 3, indicating an almost angle-independent performance up to $\theta = 60$ degrees for the resonant peak. Such insensitivity to incident angle provides convenience in practical applications. However, the co-polarization transmission coefficient t_{vv} of v -polarized wave does not coincide well with t_{uu} of u -polarized wave, and the discrepancy between t_{vv} and t_{uu} becomes more and more obvious with the increasing of incident angle, which implies that asymmetric transmission of circular polarization waves is occurred [36, 40]. Furthermore, when the incident angle θ is 60 degrees, we can see that $t_{uv} = 0.85$, $t_{uu} = 0.05$, $t_{vv} = 0.05$, $t_{vu} = 0.02$ at frequency of 20.5 GHz, except the transmitted energy, and nearly all of energy is reflected due to the small loss tangent of the dielectric.

3.3. Physical Mechanism of the Polarization Conversion

For convenience, three layers of the proposed polarization converter were marked as M1, M2 and M3, respectively. In our design, the three-layer MM can form two isolated Fabry-Pérot-like resonant cavities:

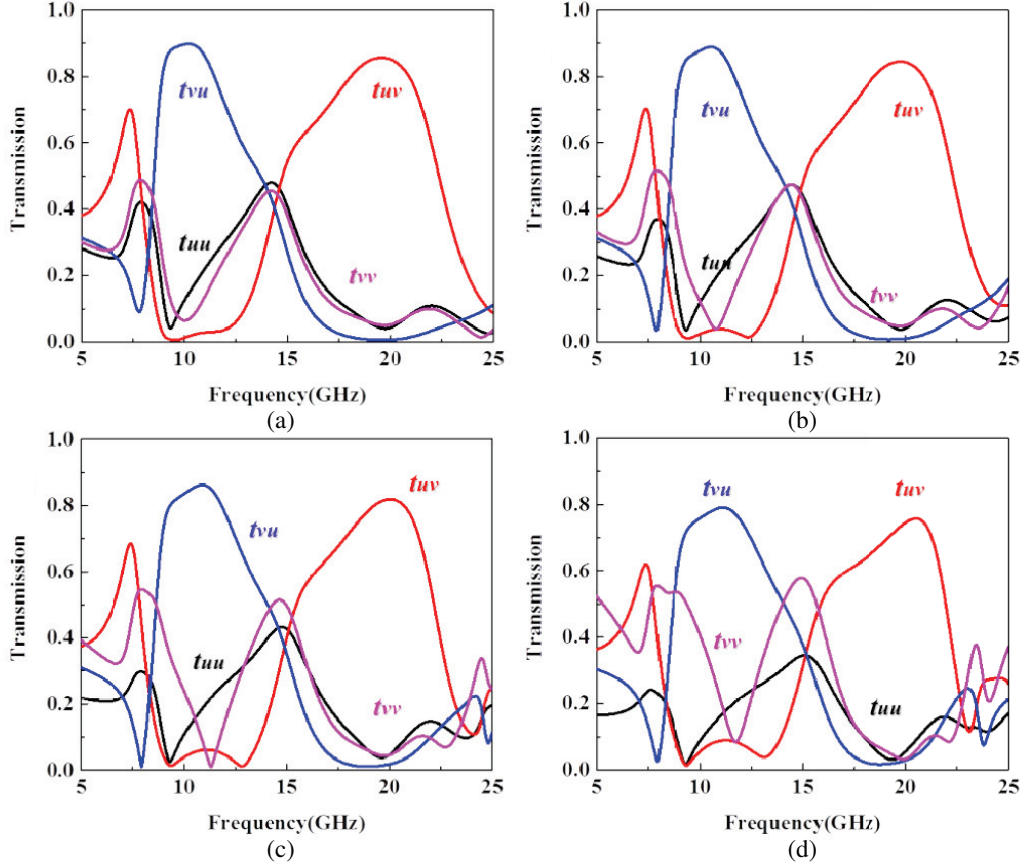


Figure 3. Transmission coefficients of linearly polarized waves at different incidence angle. (a) 15° , (b) 30° , (c) 45° and (d) 60° .

the first Fabry-Pérot-like resonant cavity constituted the layer M1 and M2, the second Fabry-Pérot-like resonant cavity constituted the layer M2 and M3. The electric field distributions of the two resonant cavities are shown in Figs. 4(a) and (b), and the schematic of the cavity like MM is shown in Fig. 4(c). The incident wave can be either u -polarized or v -polarized and the resonant frequency of 9.7 GHz is considered.

In Figs. 4(a) and (b), as the incident wave comes into the first Fabry-Pérot-like resonant cavity, the EM wave travels back and front between the top DSRR layer and middle cut-wire layer, leading to a constructive interference between the multiple polarization couplings, and the polarization of the transmission wave is thereby rotated by 135° (colorful arrows in Fig. 4). Subsequently, the polarization of the transmission wave is further rotated by about 135° when it penetrates through the second Fabry-Pérot-like resonant cavity. As a consequence, the u -polarized incident wave is efficiently transmitted to v -polarized wave. For the v -polarized incidence, a similar case also exists. According to the above analysis results, the physical mechanism for the giant and broadband AT effect of the proposed MM is shown in Fig. 4(c). The metallic DSRR are responsible for polarization conversion, including the processes of transmission and reflection, the cut-wire acts as a linear polarization selector polarization with an electric field parallel to the wires is fully transmitted while the perpendicular one is totally reflected. Hence, the cut-wire forms two independent cavities with two DSRR, which largely enhance the asymmetric transmission parameter. Our investigations indicate that the design of Fabry-Pérot-like resonant cavity can explain why the MM could achieve broadband polarization converter and asymmetric transmission of linearly polarized wave.

To further understand the physical mechanism of polarization conversion, electric field distributions along forward incident direction at resonant frequencies of 9.7 GHz and 19.27 GHz are presented in Fig. 5.

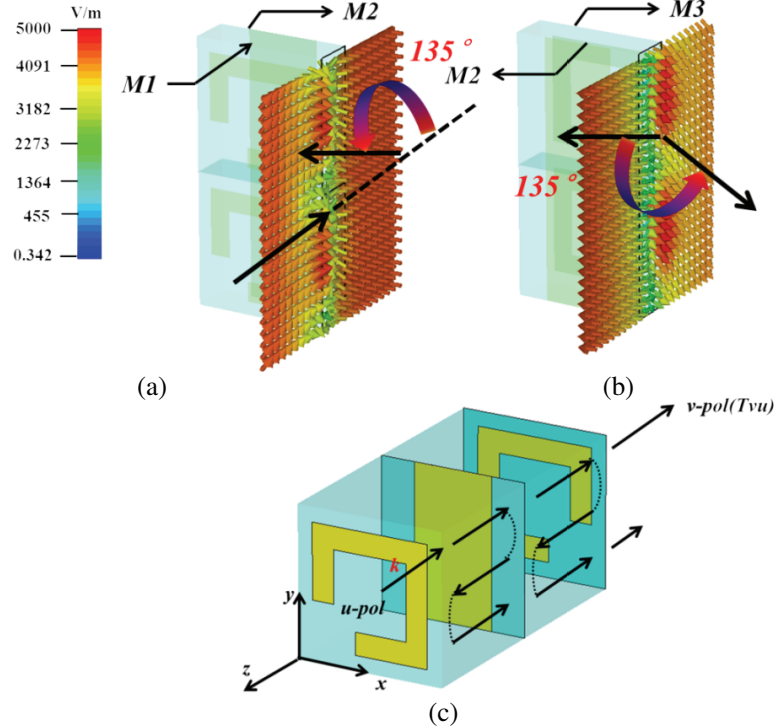


Figure 4. Electric field distribution for the first Fabry-Pérot-like resonant cavity; (b) Electric field distribution for the second Fabry-Pérot-like resonant cavity; (c) Schematic of the Fabry-Pérot-like interference effect.

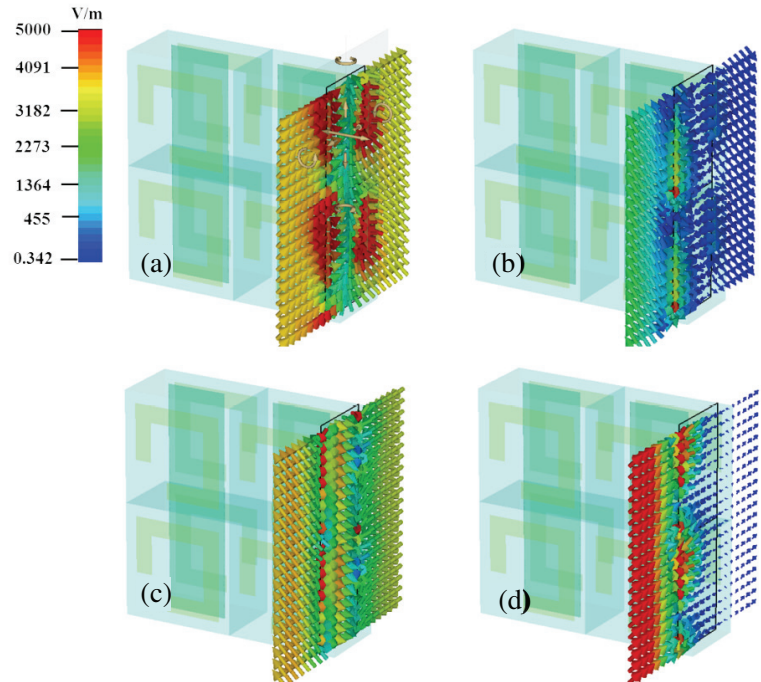


Figure 5. Electric field distributions along forward incident direction (a) u -polarized, 9.7 GHz; (b) v -polarized, 9.7 GHz; (c) u -polarized, 19.27 GHz; (d) v -polarized, 19.27 GHz. (a) at normal incidence. (b) at 60° oblique incidence.

For the proposed MM, the electric fields distributions for u -polarized and v -polarized incident waves at 9.7 GHz are shown in Fig. 5(a) and Fig. 5(b), respectively, which is clear that the u -polarized incident wave is transformed into a v -polarized output wave at this frequency, but reflects most of the v -polarized wave as depicted in Fig. 5(b), while at 19.27 GHz, v -polarized wave is almost completely transmitted to v -polarized wave, and the incident u -polarized wave is completely blocked through the structure as shown in Figs. 5(c) and (d). By observation of the electric field magnitudes as shown in Figs. 5(b) and (d), we can see that transmission t_{vv} is about 0.05 at frequency of 9.7 GHz, and t_{uu} is about 0.1 at frequency of 19.27 GHz. These results coincide with the analysis results in Fig. 2.

Moreover, surface current distributions on metal patches of all the three layers at the resonant frequency of 9.7 GHz are also considered. Just as shown in Fig. 6, the brown, red and purple arrows represent the surface current direction of top DSRR layer, middle cut-wire layer and bottom DSRR layer, respectively. As we know, the coupling effect between electric and magnetic fields plays an

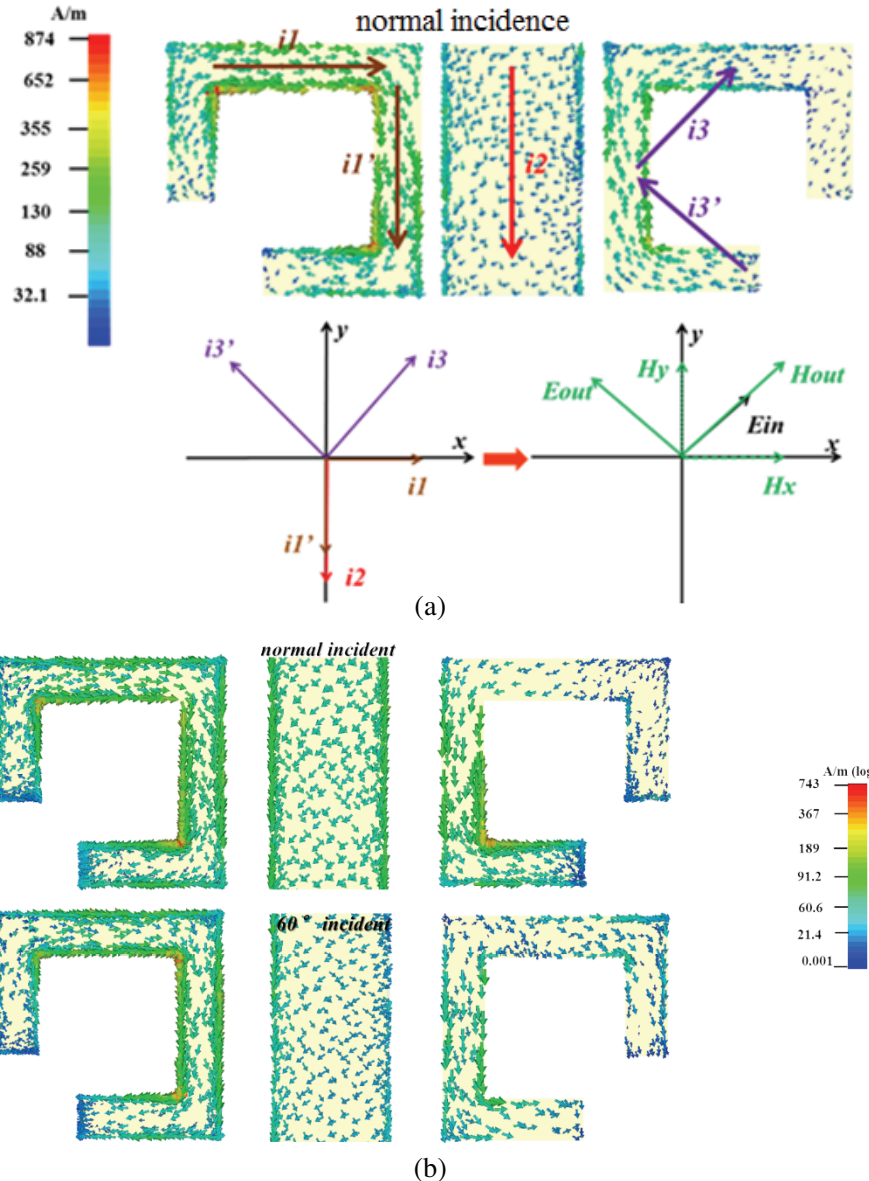


Figure 6. Surface current distributions on metal patches of all the three layers at the resonant frequency 9.7 GHz. (a) at normal incidence, (b) at 60° oblique incidence.

important role in a chiral or anisotropic MM. It is observed from Fig. 6 that the x component H_x is generated by the anti-symmetric currents decomposed in x direction and y component H_y generated by the symmetric currents in y direction. Then we can obtain the total magnetic field H_{out} , which is parallel to the incident electric field E_{in} . Thus the E_{in} and H_{out} generate the cross-coupling effect and leads to a u -to- v cross-polarization and most energy of the u -polarized incident wave is transformed with a 90° rotation at resonant frequency of 9.7 GHz.

Next, the physical explanation about angle independent of the structure will be considered. The surface electric current distributions of the proposed multi-layers structure are obtained for the normal incidence and 60 degree oblique incidence at the resonant frequency of 9.7 GHz, just as shown in Fig. 6. It is clear that the surface current distributions coincide well at two different incident angles, which could be understood as that the mechanism of polarization conversion in oblique incident is the same as normal.

4. CONCLUSION

In summary, we have proposed a three-layer transmission polarization converter MM both numerically and experimentally. The proposed polarization converter can accomplish high efficiency and broad bandwidth for the linear polarization waves. Subsequently, the polarization converter has a dual-band asymmetric transmission in two opposite directions, distinct from the MMs previously reported which only show a single-band asymmetric transmission effect for one polarization. Furthermore, the proposed polarization converter can maintain the same polarization conversion effect when the incidence angle increases from 0° to 60° for both u - and v -polarized waves. Strong asymmetric transmission effect of linear polarization waves along two opposite propagation directions occurs, and the proposed MM can reveal a perfect polarization conversion with over 85% conversion efficiency for both u - and v -polarized waves. These two separated asymmetric transmission passbands have a function of selective polarization filter, which can be switched on/off by changing the polarization state of incident waves, and then the electric field in the Fabry-Pérot-like resonant cavity and surface current distribution is applied to demonstrate physical mechanisms of the polarization conversion.

ACKNOWLEDGMENT

This research was partially supported by the National Natural Science Foundation of China (Grant No. 51301031), and Supported by Program for Changjiang Scholars and Innovative Research Team in University (PCSIRT).

REFERENCES

1. Fedotov, V. A., P. L. Mladyonov, S. L. Prosvirnin, A. V. Rogacheva, Y. Chen, and N. I. Zheludev, “Asymmetric propagation of electromagnetic waves through a planar chiral structure,” *Phys. Rev. Lett.*, Vol. 97, No. 16, 167401, 2006.
2. Ma, X., C. Huang, M. Pu, Y. Wang, and Z. Zhao, “Dual-band asymmetry chiral metamaterial based on planar spiral structure,” *Appl. Phys. Lett.*, Vol. 101, 161901, 2012.
3. Mutlu, M., A. E. Akosman, A. E. Serebryannikov, and E. Ozbay, “Asymmetric transmission of linearly polarized waves and polarization angle dependent wave rotation using a chiral metamaterial,” *Opt. Express*, Vol. 19, No. 15, 14290–14299, 2011.
4. Ji, R., S. W. Wang, X. Liu, and W. Lu, “Giant and broadband circular asymmetric transmission based on two cascading polarization conversion cavities,” *Nanoscale*, Vol. 8, No. 15, 8189–8194, 2016.
5. Singh, R., E. Plum, C. Menzel, C. Rockstuhl, A. K. Azad, R. A. Cheville, F. Lederer, W. Zhang, and N. I. Zheludev, “Terahertz metamaterial with asymmetric transmission,” *Phys. Rev. B*, Vol. 80, No. 15, 153104, 2009.

6. Ozer, Z., F. Dincer, M. Karaaslan, et al., "Asymmetric transmission of linearly polarized light through dynamic chiral metamaterials in a frequency regime of gigahertz-terahertz," *Optical Engineering*, Vol. 53, No. 7, 075109–075109, 2014.
7. Wang, F., A. Chakrabarty, F. Minkowski, K. Sun, and Q.-H. Wei, "Polarization conversion with elliptical patch nanoantennas," *Appl. Phys. Lett.*, Vol. 101, 023101, 2012.
8. Liu, L., C. Caloz, and T. Itoh, "Dominant mode leaky-wave antenna with backfire-to-endfire scanning capability," *Elec. Letters*, Vol. 38, No. 23, 1414–1416, 2002.
9. Landy, N. I., S. Sajuyigbe, J. J. Mock, D. R. Smith, and W. J. Padilla, "Perfect metamaterialabsorber," *Phys. Rev. Lett.*, Vol. 100, No. 20, 207402, 2008.
10. Kundtz, N. and D. R. Smith, "Extreme-angle broadband metamaterial lens," *Nat. Mater.*, Vol. 9, 129–132, 2010.
11. Schurig, D., J. J. Mock, B. J. Justice, S. A. Cummer, J. B. Pendry, A. F. Starr, and D. R. Smith, "Metamaterial electromagnetic cloak at microwave frequencies," *Science*, Vol. 314, No. 5801, 977–980, 2006.
12. Huang, L., X. Chen, H. Mühlenbernd, G. Li, B. Bai, Q. Tan, G. Jin, T. Zentgraf, and S. Zhang, "Dispersionless phase discontinuities for controlling light propagation," *Nano Lett.*, Vol. 12, No. 11, 5750–5755, 2012.
13. Altintas, O., E. Unal, O. Akgol, et al., "Design of a wide band metasurface as a linear to circular polarization converter," *Modern Physics Letters B*, Vol. 31, No. 30, 1750274, 2017.
14. Cheng, Y., Y. Nie, X. Wang, et al., "An ultrathin transparent metamaterial polarization transformer based on a twist-split-ring resonator," *Applied Physics A*, Vol. 111, No. 1, 209–215, 2013.
15. Cheng, Y., C. Wu, Z. Z. Cheng, et al., "Ultra-compact multi-band chiral metamaterial circular polarizer based on triple twisted split-ring resonator," *Progress In Electromagnetics Research*, Vol. 155, 105–113, 2016.
16. Zhao, J. C. and Y. Z. Cheng, "Ultra-broadband and high-efficiency reflective linear polarization convertor based on planar anisotropic metamaterial in microwave region," *Optik-International Journal for Light and Electron Optics*, Vol. 136, 52–57, 2017.
17. Fang, C., Y. Cheng, Z. He, et al., "Design of a wideband reflective linear polarization converter based on the ladder-shaped structure metasurface," *Optik-International Journal for Light and Electron Optics*, Vol. 137, 148–155, 2017.
18. Hao, J., Y. Yuan, L. Ran, T. Jiang, J. A. Kong, C. T. Chan, and L. Zhou, "Manipulating electromagnetic wave polarizations by anisotropic metamaterials," *Phys. Rev. Lett.*, Vol. 99, No. 6, 063908, 2007.
19. Ye, Y. and S. He, "90° polarization rotator using a bilayered chiral metamaterial with giant optical activity," *Appl. Phys. Lett.*, Vol. 96, No. 20, 203501, 2010.
20. Grady, N. K., J. E. Heyes, D. R. Chowdhury, Y. Zeng, M. T. Reiten, A. K. Azad, A. J. Taylor, D. A. R. Dalvit, and H.-T. Chen, "Terahertz Metamaterials for Linear Polarization Conversion and Anomalous Refraction," *Science*, Vol. 340, No. 6138, 1304–1307, 2013.
21. Zhu, W., I. D. Rukhlenko, Y. Huang, G. Wen, and M. Premaratne, "Wideband giant optical activity and negligible circular dichroism of near-infrared chiral metamaterial based on a complementary twisted configuration," *J. Opt.*, Vol. 15, No. 12, 125101, 2013.
22. Serebryannikov, A. E., M. Beruete, M. Mutlu, and E. Ozbay. "Multiband one-way polarization conversion in complementary split-ring resonator based structures by combining chirality and tunneling," *Opt. Express*, Vol. 23, No. 10, 13517–13529, 2015.
23. Markovich, D., A. Andryieuski, M. Zalkovskij, R. Malureanu, and A. Lavrinenko, "Metamaterial polarization converter analysis: limits of performance," *Appl. Phys. B*, Vol. 112, No. 2, 143–152, 2013.
24. Serebryannikov, A. E., M. Mutlu, and E. Ozbay, "Dielectric inspired scaling of polarization conversion subwavelength resonances in open ultrathin chiral structures," *Appl. Phys. Lett.*, Vol. 107, No. 22, 221907, 2015.

25. Dong, G. X., H. Y. Shi, S. Xia, et al., "Ultra-broadband and high-efficiency polarization conversion metasurface with multiple plasmon resonance modes," *Chinese Physics B*, Vol. 25, No. 8, 084202, 2016.
26. Zhao, J. C. and Y. Z. Cheng, "A high-efficiency and broadband reflective 90° linear polarization rotator based on anisotropic metamaterial," *Applied Physics B*, Vol. 122, No. 10, 255, 2016.
27. Cheng, Y. Z., C. Fang, X. S. Mao, et al., "Design of an ultrabroadband and high-efficiency reflective linear polarization convertor at optical," *IEEE Photonics Journal*, Vol. 8, No. 6, 1–9, 2016.
28. Aieta, F., P. Genevet, N. Yu, M. A. Kats, Z. Gaburro, and F. Capasso, "Out-of-plane reflection and refraction of light by anisotropic optical antenna metasurfaces with phase discontinuities," *Nano Lett.*, Vol. 12, No. 3, 1702–1706, 2012.
29. Schwanecke, A. S., V. A. Fedotov, V. V. Khardikov, S. L. Prosvirnin, Y. Chen, and N. I. Zheludev, "Nanostructured metal film with asymmetric optical transmission," *Nano Lett.*, Vol. 8, 2940, 2008.
30. Menzel, C., C. Helgert, C. Rockstuhl, E. B. Kley, A. Tunnermann, T. Pertsch, and F. Lederer, "Asymmetric transmission of linearly polarized light at optical metamaterials," *Phys. Rev. Lett.*, Vol. 104, 253902, 2010.
31. Wei, Z., Y. Cao, Y. Fan, X. Yu, and H. Li, "Broadband polarization transformation via enhanced asymmetric transmission through arrays of twisted complementary split-ring resonators," *Appl. Phys. Lett.*, Vol. 99, No. 22, 221907, 2011.
32. Stolarek, M., D. Yavorskiy, R. Kotyński, C. J. Zapata Rodríguez, J. Lusakowski, and T. Szoplik, "Asymmetric transmission of terahertz radiation through a double grating," *Opt. Lett.*, Vol. 38, No. 6, 839–841, 2013.
33. Mutlu, M., A. E. Akosman, A. E. Serebryannikov, and E. Ozbay, "Diodelike asymmetric transmission of linearly polarized waves using magnetoelectric coupling and electromagnetic wave tunneling," *Phys. Rev. Lett.*, Vol. 108, No. 21, 213905, 2012.
34. Zhang, L., P. Zhou, H. Chen, H. Lu, H. Xie, L. Zhang, E. li, J. Xie, and L. Deng, "Ultrabroadband Design for Linear Polarization Conversion and Asymmetric Transmission Crossing X-and K-Band," *Sci. Reports*, Vol. 10, No. 1038, 33826, 2016.
35. Cheng, Y. Z., R. Z. Gong, and L. Wu, "Ultra-broadband linear polarization conversion via diode-like asymmetric transmission with composite metamaterial for teraherze waves," *Plasmonics*, Vol. 12, No. 4, 1113–1120, 2017.
36. Kang, M., J. Chen, H. X. Cui, Y. Li, and H. T. Wang, "Asymmetric transmission for linearly polarized electromagnetic radiation," *Opt. Express*, Vol. 19, No. 9, 8347–8356, 2011.
37. Shi, J. H., X. C. Liu, S. W. Yu, T. T. Lv, Z. Zhu, H. F. Ma, and T. J. Cui, "Dual-band asymmetric transmission of linear polarization in bilayered chiral metamaterial," *Appl. Phys. Lett.*, Vol. 102, No. 19, 191905, 2013.
38. Wang, Y. H., J. Shao, J. Li, M. J. Zhu, J. Q. Li, L. Zhou, and Z. G. Dong, "Broadband asymmetric transmission by rotated bilayer cross-shaped metamaterials," *J. Phys. D: Appl. Phys.*, Vol. 48, 485306, 2015.
39. Wang, Y. H., J. Shao, J. Li, et al., "Broadband high-efficiency transmission asymmetry by a chiral bilayer bar metastructure," *J. Appl. Phys.*, Vol. 117, No. 17, 173102-1–173102-7, 2015.
40. Liu, D. J., Z. Y. Xiao, X. L. Ma, and Z. H. Wang, "Asymmetric transmission of linearly and circularly polarized waves in metamaterial due to symmetry-breaking," *Appl. Phys. Express*, Vol. 8, No. 5, 052001, 2015.